Available online at www.sciencedirect.com

ScienceDirect

journal homepage: http://www.elsevier.com/locate/rpor

Original research article

Evaluation of raw-data-based and calculated electron density for contrast media with a dual-energy CT technique

Daisuke Kawahara[a,b,*], *Shuichi Ozawa*[c,d], *Kazushi Yokomachi*[a], *Toru Higaki*[e], *Takehiro Shiinoki*[c,f], *Yoshimi Ohno*[a], *Yuji Murakami*[c], *Kazuo Awai*[f], *Yasushi Nagata*[c,d]

[a] *Radiation Therapy Section, Division of Clinical Support, Hiroshima University Hospital, Hiroshima, 734-8551, Japan*

[b] *Medical and Dental Sciences Course, Graduate School of Biomedical & Health Sciences, Hiroshima University, Hiroshima, 734-8551, Japan*

[c] *Department of Radiation Oncology, Institute of Biomedical & Health Sciences, Hiroshima University, Hiroshima, 734-8551, Japan*

[d] *Hiroshima High-Precision Radiotherapy Cancer Center, Hiroshima, 732-0057, Japan*

[e] *Departments of Diagnostic Radiology and Radiology, Hiroshima University, Hiroshima, 734-8551, Japan*

[f] *Department of Radiation Oncology, Graduate School of Medicine, Yamaguchi University, Yamaguchi, 753-8511, Japan*

ARTICLE INFO

Article history:
Received 19 December 2018
Received in revised form 7 May 2019
Accepted 30 July 2019
Available online 20 August 2019

Keywords:
Dual-energy CT
Relative electron density
CT number
Contrast material
Beam hardening

ABSTRACT

Objectives: The aim of the current study is to evaluate the accuracy and the precision of raw-data-based relative electron density (RED_{raw}) and the calibration-based RED (RED_{cal}) at a range of low-RED to high-RED for tissue-equivalent phantom materials by comparing them with reference RED (RED_{ref}) and to present the difference of RED_{raw} and RED_{cal} for the contrast medium using dual-energy CT (DECT).

Methods: The RED_{raw} images were reconstructed by raw-data-based decomposition using DECT. For evaluation of the accuracy of the RED_{raw}, RED_{ref} was calculated for the tissue-equivalent phantom materials based on their specified density and elemental composition. The RED_{cal} images were calculated using three models: Lung-Bone model, Lung-Ti model and Lung-Ti (SEMAR) model which used single-energy metal artifact reduction (SEMAR). The difference between RED_{raw} and RED_{cal} was calculated.

Results: In the titanium rod core, the deviations of RED_{raw} and RED_{cal} (Lung-Bone model, Lung-Ti model and Lung-Ti model with SEMAR) from RED_{ref} were 0.45%, 50.8%, 15.4% and 15.0%, respectively. The largest differences between RED_{raw} and RED_{cal} (Lung-Bone model, Lung-Ti model and Lung-Ti model with SEMAR) in the contrast medium phantom were

* *Corresponding author at*: Radiation Therapy Section, Department of Clinical Support, Hiroshima University Hospital, 1-2-3 Kasumi, Minami-ku, Hiroshima City 734-8551, Japan.
E-mail address: daika99@hiroshima-u.ac.jp (D. Kawahara).

https://doi.org/10.1016/j.rpor.2019.07.013

8.2%, −23.7%, and 28.7%, respectively. However, the differences between RED_{raw} and RED_{cal} values were within 10% at 20 mg/ml. The standard deviation of the RED_{raw} was significantly smaller than the RED_{cal} with three models in the titanium and the materials that had low CT numbers.

Conclusion: The RED_{cal} values could be affected by beam hardening artifacts and the RED_{cal} was less accurate than RED_{raw} for high-Z materials as titanium.

Advances in knowledge: The raw-data-based reconstruction method could reduce the beam hardening artifact compared with image-based reconstruction and increase the accuracy for the RED estimation in high-Z materials, such as titanium and iodinated contrast medium.

1. Background

In radiation therapy, uncertainties from multiple sources that influence the delivery of the prescribed dose to the target could lead to potential errors in dose delivery. At the target definition step, sources of uncertainties include target motion, patient set up errors, organ motion, and delineation of the target volume. On treatment planning systems, the dose calculation algorithms and computed tomography (CT) data which can correct tissue heterogeneity in radiotherapy treatment plans are included. Recently, the accuracy of patient dose calculations has been improved by the use of the kernel-based superposition/convolution and Monte Carlo algorithms.[1] CT images contain CT numbers that can be used to correct tissue heterogeneity. For accurate dose calculations, treatment planning systems need a correctly calibrated relationship between the CT numbers and electron density (ED).[2]

CT imaging is used for radiation therapy planning. For the accuracy of patient dose calculation, conversion of the CT number into an ED relative to water (RED) is one of the main steps.[3] The CT number–RED conversion is currently executed using tissue-equivalent materials with known REDs in a calibration phantom.[4] The tissue-equivalent materials could show different CT numbers because of the scanning and reconstruction settings. Moreover, the CT number and RED value cannot be interrelated by a simple one-to-one correspondence.[5,6] To resolve the problem of the CT number–RED conversion, Schneider et al. proposed the stoichiometric calibration method.[7] In the stoichiometric calibration method, a set of materials with known chemical compositions and densities is scanned by a CT scanner. The measured CT numbers are fitted to a theoretical equation, and then the CT numbers of real tissues are estimated using the fitted parameters and tabulated composition data. Although the stoichiometric calibration method works better than the conventional tissue–substitute calibration, the CT numbers depend on the ED and effective atomic numbers, and using single energy CT (SECT) these two parameters cannot be separately estimated.

Dual-energy CT (DECT) acquires CT data sets at two different X-ray spectra to obtain material-specific information using material decomposition algorithms that analyze the change in tissue attenuation.[8] Saito proposed calculated RED (RED_{cal}), which is a conversion of the energy-subtracted CT number to a RED (ΔHU–RED).[9] The linearity of the ΔHU–RED plot was confirmed experimentally using a clinical dual-source CT scanner with an ED phantom.[10] Saito performed DECT image simulations and predicted a single linear relationship between the change of CT number and the RED over a wide range of RED values from air to aluminum. However, they did not show the data of materials with a higher density than aluminum and of contrast medium. Contrast medium is often used to obtain an accurate delineation of tumors or other diseases. In addition, DECT can obtain various other data, such as effective atomic numbers, mono-energy CT numbers, and REDs.[11] In a current study, a single-source CT scanner with switching voltages implemented by Toshiba in the Aquilion One (Toshiba Medical Systems Corporation, Tokyo, Japan) was used.[12] An advantage of this DECT approach is a perfect alignment of the subsequent images, allowing material decomposition to be performed in raw data space, using sinogram-based reconstruction. Other approaches use image-based reconstruction for material decomposition. Moreover, Meinel et al. showed that raw-data-based relative electron density (RED_{raw}) data created by the Toshiba Aquilion One reduced the effect of the metal beam hardening artifact based on the CT image.[13,14] Accordingly, DECT by Toshiba Aquilion One that reduces the metal artifacts can improve the accuracy of material decomposition. Consequently, the RED_{raw} can be used for treatment planning without using a CT number–RED calibration table if the accuracy of the RED_{raw} is adequate.

The aim of the current study is to evaluate the accuracy and the precision of RED_{raw} and the calibration fit of RED_{cal} at a range of low-RED to high-RED for tissue-equivalent phantom materials by comparing them with reference RED (RED_{ref}) and to present the difference of RED_{raw} and RED_{cal} for the contrast medium using DECT.

2. Materials and methods

Two different phantoms were used (Fig. 1), an ED phantom (Model 062M; Computerized Imaging Reference Systems; CIRS, Inc., Norfolk, Virginia, USA) and an acrylic phantom into which different concentrations of iodinated contrast medium were inserted. The ED phantom contained several tissue-equivalent inserts: lung inhale, lung exhale, adipose, breast, water, muscle, liver, trabecular bone (200 mg/cm^3 hydroxyapatite), dense bone (800 mg/cm^3 hydroxyapatite), dense bone (1250 mg/cm^3 hydroxyapatite), and titanium, whose atomic compositions and densities are well known and provided by the

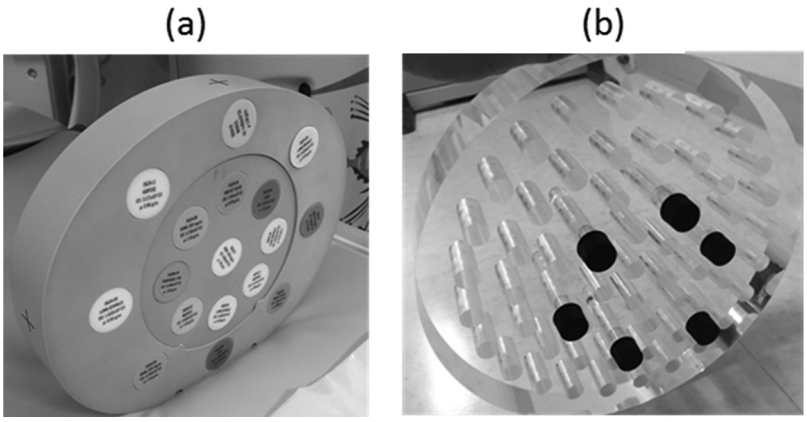

Fig. 1 – (a) Electron density phantom model 062 M and (b) acrylic phantom with different concentrations of iodinated contrast medium inserted.

manufacturer. For the acrylic phantom, syringes were filled with solutions prepared by diluting iodine contrast medium (Omnipaque 300, GE Healthcare, Princeton, New Jersey, USA) with water to predetermined concentrations of 0, 1, 2, 3, 4, 5, 6, 7, 8, 9, 10, 20, 40, 60, 90, and 130 mg iodine per ml.

2.1. *CT and RED$_{raw}$ images reconstructed using DECT*

DECT scans were acquired with the CT scanner (Aquilion One; Toshiba, Tokyo, Japan) at Hiroshima University Hospital. CT scans were performed at tube voltages of 80 and 135 kV. Tube currents of 800 and 200 mA were used for 80 and 135 kV, respectively. The time to switch the tube voltage between 80 and 135 kV was 0.4 s. The other scanning parameters were rotation time of 1.0 s, slice thickness of 0.5 mm, and field of view of 400 mm. The total number of slices was 80, and the middle of each slice was analyzed in all cases. The Aquilion One can use a metal artifact reduction algorithm called single-energy metal artifact reduction (SEMAR).[15] SEMAR uses a modified sinogram inpainting technique to reduce metal artifacts. The CT images were reconstructed with and without SEMAR.

The CT number of a material is defined by

$$\text{CT number} = \left[\frac{\mu - \mu_{\text{water}}}{\mu_{\text{water}} - \mu_{\text{air}}}\right] \times 1000 \quad (1)$$

where μ is linear attenuation coefficient for the material, and μ_{water} and μ_{air} are the attenuation coefficients of water and air, respectively.

The unit for CT numbers is Hounsfield units (HU); by definition, water is zero HU and air is −1000 HU.

In the CT energy range, the linear attenuation coefficient μ of for the photon energy E can be described by photoelectric absorption and Compton scattering.[15] The simplified formula is

$$\mu(E) = m_p f_p(E) + m_c f_c(E) \quad (2)$$

where m_p and m_c are constants that depend on the material, and f_p and f_c are functions that depend on the energy, E, for the photoelectric absorption and Compton scattering, respectively. The photoelectric absorption depends on both the effective atomic number and the relative electron density of the material, while the Compton scattering does not depend explicitly on the effective atomic number, Eq. (2) can therefore be reformulated as follows:

$$\mu(E) = f(\rho_e, Z_{\text{eff}}, E) + f(\rho_e, Z_{\text{eff}}) \quad (3)$$

where ρ_e is the RED_{raw} and Z_{eff} is the effective atomic number. In DECT processing, a linear attenuation coefficient could be showed by 2 basis materials as follows:

$$\mu(E) = \mu_1(E)c_1 + \mu_2(E)c_2 \quad (4)$$

where coefficients c_1 and c_2 are vary spatial and independent of energy. The $\mu_1(E)$ and $\mu_2(E)$ are known functions of photon energy.

By solving Eqs. (3) and (4), the RED and Z_{eff} can be obtained. The software package ImageJ (National Institutes of Health, Bethesda, Maryland, USA) was employed to analyze the CT and RED_{raw} images. This is the basis for the sinogram-based reconstruction, which is implemented in the CT scanner. That is, the RED_{raw} images are directly obtained from the reconstruction and not from a post-process, unlike the method described in the next section. The standard deviation (SD) of CT numbers and the average values of RED_{raw} values were measured within a manually drawn region of interest (ROI) using ImageJ. Circular ROIs were drawn to cover an area as large as possible within each of the materials.

2.2. *RED$_{cal}$ calculated by the ΔHU–RED conversion method using DECT*

RED_{cal} images were calculated using the ΔHU–RED conversion method proposed by Saito[9] which applies reconstructed CT images. The RED can be expressed by the weighted subtraction of linear attenuation coefficients measured at two different energies.[16] Saito introduced a dual-energy subtracted quantity, ΔHU, into the RED calibration, which is defined as

$$\Delta\text{HU} = (1+\alpha)\text{HU}_H - \alpha\text{HU}_L, \quad (5)$$

where HU_H and HU_L are the CT number in Hounsfield units for high-kV and low-kV scans, and α is the weighting factor for the subtraction. For materials with lower effective atomic numbers (as in human tissues), α could be regarded as a single, material-independent parameter specified only by the mean energies of the high-kV and low-kV spectra of the CT scanner. Thus, the relationship between ΔHU and RED is an invariably linear relation. The scanner-specific α is numerically determined using a ΔHU–RED data set to maximize the coefficient of determination, r^2, by a least-squares fit to the linear function. The RED_{cal}, defined as ρ_e^{cal} for ΔHU with each α using Eq. (5), is fitted as follows:

$$\rho_e^{cal} = a\frac{\Delta HU}{1000} + b \quad (6)$$

In this fitting process, the coefficient of determination r^2 is evaluated and, then, we determine the optimal α that provides the largest r^2. In the ideal case, r^2, slope a, and intercept b are unity. In order to determine the weighting factor α, a, and b, we first performed the ΔHU–RED conversion for the ED phantom using their measured CT numbers and manufacturer specified RED. In the current study, we used two types of the calibration method using the ED phantom. For one calibration, RED values range from 0.190 (lung inhale) to 1.695 (solid dense bone (1250 mg/cm^3)) were used for ΔHU–RED conversion (Lung-Bone model). For the human tissue materials, only this method was used. For the other, the RED values ranging from 0.190 (lung inhale) to 3.735 (titanium rod core) were used for ΔHU–RED conversion (Lung-Ti model). Additional, RED_{cal} value ranges from lung inhale to titanium with SEMAR was used for ΔHU–RED conversion (Lung-Ti model with SEMAR). These two latter models corresponded to materials with a higher density, such as metal and contrast medium. The determined conversion parameters of α, a, and b were used for the calibration.

2.3. *Evaluation of RED_{raw} and RED_{cal} values*

Only for the tissue-equivalent materials in the ED phantom reference values for the RED was provided. Therefore, the accuracy of the RED_{raw} and the RED_{cal} was first established in this phantom by using the vendor specified values for the RED as a reference (RED_{ref}). In contrast, no ground truth reference RED could be accurately calculated for the contrast medium. Instead, only the difference between RED_{raw} and RED_{cal} was calculated here. But as seen in Table 1, the RED_{raw} provided the most accurate RED estimates for the ED phantom and at the same time the standard deviation for the RED_{raw} values was lower than for the RED_{cal}. Therefore, the RED_{raw} values were seen as the reference values for the RED estimates in the contrast media.

3. Results

3.1. *RED_{raw} and RED_{cal} using the CT–ED phantom*

Fig. 2 shows r^2 as a function of the weighting factor α used in the calculation of RED_{cal}, Eq. (5). Here, the weighting factor α was set to 0.85 for Lung-Ti model with and without SEMAR and 1.05 for Lung-Bone model because these provided the largest r^2. The corresponding RED_{cal}, defined as the ρ_e^{cal} value, was fitted to the data. Fig. 3(a) shows the CT number–RED and ΔHU–RED plots and a magnified portion of the soft-tissue region between $\pm$100 HU is shown in Fig. 3(b). The results of the a and b, for the fitted curve were 1.000 and 0.987 for the Lung-Bone model, 0.900 and 0.974 for Lung-Ti model, and 0.900 and 0974 for Lung-Ti model with SEMAR, respectively.

Table 1 shows the deviations from the RED_{ref}, and the standard deviation (SD) of the RED_{raw} and RED_{cal} (Lung-Bone, and Lung-Ti and Lung-Ti with SEMAR) in the ED phantom. The deviation of RED_{raw} from RED_{ref} was at most 3.4% from lung inhale to titanium. The SDs of RED_{raw} were 0.03 at a range of lung inhale to titanium. The differences of RED_{cal} (Lung-Bone, Lung-Ti, and Lung-Ti with SEMAR) from RED_{ref}, i.e., in the ED phantom, were within −3.8%, −5.0%, and −5.0%, respectively, from lung inhale to solid dense bone. However, in the titanium rod core contained in the ED phantom, the deviations of RED_{raw} and RED_{cal} (Lung-Bone, Lung-Ti, and Lung-Ti with SEMAR) from RED_{ref} were −0.5%, 50.8%, 15.4% and 13.0%, respectively. The SD of the RED_{raw} was significantly lower than the RED_{cal} in the breast, adipose, liver, muscle and titanium. From these results, the RED_{raw} was more accurate than the RED_{cal} (Lung-Bone, and Lung-Ti and Lung-Ti with SEMAR) at a range of low-RED to high-RED. Therefore, the RED_{raw} was defined as the reference values using the acrylic phantom in which were inserted different concentrations of iodinated contrast medium (Section 2.3).

3.2. *RED_{raw} and RED_{cal} for iodinated contrast medium*

Table 2 shows the results of the average and the SD of RED_{raw} and RED_{cal}, and the difference between the RED_{raw} and the RED_{cal} for the different concentrations of iodinated contrast medium. The RED_{raw} and RED_{cal} increased as the concentration of the contrast medium increased. The differences between RED_{cal} and RED_{raw} (Lung-Bone model, Lung-Ti model and Lung-Ti model with SEMAR), were within 10% for concentrations less than 20 mg/ml. In contrast, the maximum deviations of RED_{cal} (Lung-Bone, Lung-Ti and Lung-Ti with SEMAR) and RED_{raw} in the contrast medium phantom were 8.2%, −23.7%, and 28.7% at a concentration of 130 mg/ml. Although the RED_{cal} (Lung-Ti) increased for the concentration of the contrast medium within 0–90 mg/ml, it decreased at a concentration of 130 mg/ml. The SD for RED_{raw} was significantly lower than for RED_{cal} for low concentrations of the contrast medium.

4. Discussion

The current study investigated the accuracy of RED_{raw} and RED_{cal} using an ED phantom and provided the data of an acrylic phantom with different concentrations of contrast medium inserted. The current study showed that there was a good agreement in RED_{raw} values compared with the reference data in tissue-equivalent materials in the range of 0.190 (lung inhale) to 1.695 (solid dense bone (1250 mg/cm^3)). RED_{cal} values for titanium differed for the three models (Table 1) showing that the RED_{cal} values could be affected by beam

Table 1 – The deviation of RED_{raw} and RED_{cal} from RED_{ref}. The RED_{cal} was calculated using three models: the Lung-Bone model, the Lung-Ti model, the Lung-Ti model with SEMAR using a tissue-equivalent phantom.

	RED_{ref}	RED_{raw}			RED_{cal}(Lung-Bone)			RED_{cal} (Lung-Ti)			RED_{cal} (Lung-Ti)(SEMAR)		
		Average	SD	(Ref–Raw) Diff (%)	Average	SD	(Ref–Cal) Diff (%)	Average	SD	(Ref–Cal) Diff (%)	Average	SD	(Ref–Cal) Diff (%)
Lung (inhale)	0.19	0.19	0.03	−0.39	0.16	0.00	2.79	0.23	0.00	−4.13	0.23	0.00	−4.10
Lung (exhale)	0.49	0.51	0.03	−2.48	0.50	0.01	−1.51	0.54	0.01	−5.01	0.54	0.01	−4.98
Breast	0.98	0.98	0.03	−0.06	0.96	0.25	1.44	0.95	0.25	2.65	0.95	0.25	2.68
Adipose	0.95	0.97	0.03	−2.08	0.95	0.14	0.05	0.94	0.14	1.24	0.94	0.13	1.27
Liver	1.05	1.05	0.02	0.53	1.04	0.20	1.37	1.02	0.20	3.20	1.02	0.20	3.23
Muscle	1.04	1.04	0.03	−0.27	1.05	0.19	−0.52	1.03	0.19	1.43	1.03	0.19	1.46
Bone (200 mg/cm^3)	1.12	1.10	0.03	1.11	1.11	0.05	0.73	1.10	0.05	2.01	1.10	0.05	2.04
Bone (800 mg/cm^3)	1.45	1.42	0.03	3.38	1.46	0.02	−0.69	1.45	0.02	0.24	1.45	0.02	0.27
Bone (1250 mg/cm^3)	1.69	1.69	0.03	−0.03	1.73	0.02	−3.82	1.71	0.02	−2.08	1.71	0.02	−2.05
Ti	3.73	3.73	0.03	0.45	3.22	0.53	50.76	3.58	0.54	15.40	3.60	0.54	13.00

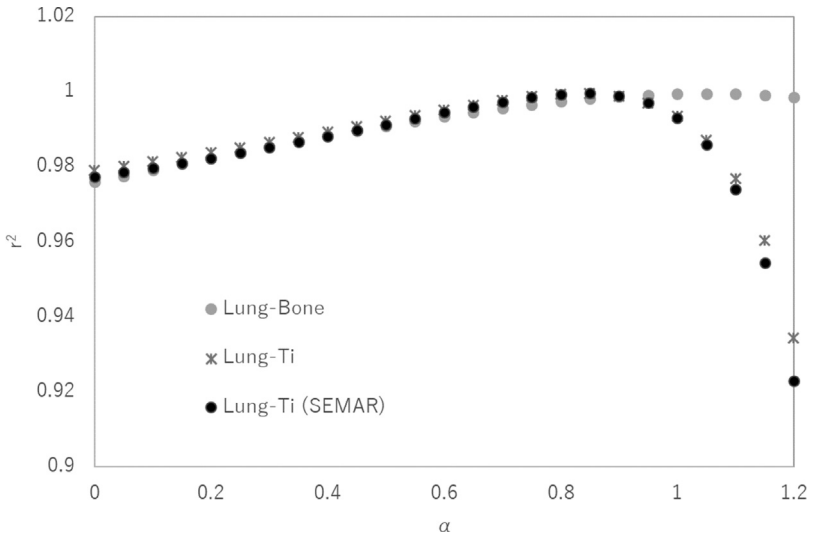

Fig. 2 – r^2 used to fit the ΔHU–RED data set to Eq. (4) as a function of the weighting factor α.

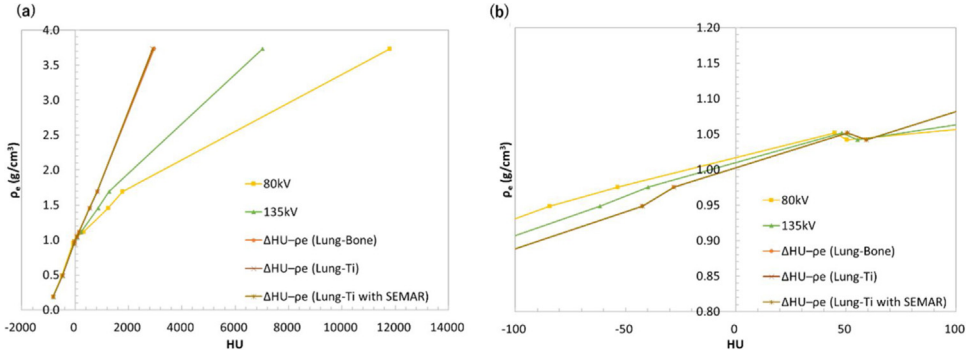

Fig. 3 – (a) CT number–RED and ΔHU–RED plots and (b) a magnified portion of the soft-tissue region between ±100 HU.

Table 2 – The average and SD of the RED_{raw} and RED_{cal} calculated in three models: the Lung-Bone model, and the Lung-Ti models, Lung-Ti models with SEMAR using the acrylic phantom with contrast medium inserted. The difference of the RED_{raw} and RED_{cal} with three models was calculated.

	RED_{raw}		RED_{cal} (Lung-Bone)			RED_{cal} (Lung-Ti)			RED_{cal} (Lung-Ti) (SEMAR)		
	Average	SD	Average	SD	(Raw–Cal) Diff (%)	Average	SD	(Raw–Cal) Diff (%)	Average	SD	(Raw–Cal) Diff (%)
1	1.00	0.05	1.00	0.32	−0.03	0.99	0.32	1.35	0.99	0.99	1.38
2	1.00	0.05	0.99	0.12	1.22	0.98	0.12	2.08	0.98	0.98	2.11
3	1.01	0.03	1.00	0.12	1.05	0.99	0.12	1.80	0.99	0.99	1.83
4	1.01	0.05	1.01	0.05	−0.46	1.00	0.05	0.18	1.00	1.00	0.21
5	1.00	0.04	1.02	0.09	−1.39	1.01	0.09	−0.80	1.01	1.01	−0.77
6	1.00	0.05	1.00	0.05	0.62	1.00	0.05	0.53	1.00	1.00	0.56
7	1.01	0.04	1.02	0.04	−1.08	1.02	0.04	−0.95	1.02	1.02	−0.92
8	1.00	0.05	1.01	0.05	−1.20	1.02	0.05	−1.62	1.02	1.02	−1.59
9	1.01	0.04	1.03	0.03	−1.55	1.03	0.03	−2.07	1.03	1.03	−2.04
10	1.00	0.04	1.02	0.02	−1.97	1.03	0.02	−2.96	1.02	1.02	−2.00
20	1.03	0.05	1.09	0.02	−5.71	1.12	0.02	−8.93	1.10	1.10	−6.53
40	1.08	0.05	1.14	0.01	−6.01	1.22	0.01	−14.40	1.24	1.24	−15.95
60	1.18	0.05	1.26	0.01	−8.44	1.39	0.01	−21.12	1.42	1.42	−23.67
90	1.32	0.05	1.34	0.02	−1.91	1.55	0.02	−22.65	1.61	1.61	−28.68
130	1.51	0.04	1.43	0.02	8.20	1.75	0.02	−23.70	1.31	1.31	20.09

hardening in materials with a higher density and high atomic number, such as titanium. Materials with a high density cannot therefore be estimated accurately using the RED_{cal} model. In contrast, the precision and the accuracy of RED_{raw} were significantly higher than the RED_{cal} at the range of low-RED to high-RED (Table 1). Owing to these results, the RED_{raw} was assumed to also give an accurate estimate in the contrast medium. Compared with the RED_{cal}, the differences were

within 10% for concentrations less than 20 mg/ml. Bae showed that the maximum iodine concentration of abdominal aorta or liver that had undergone an injection of contrast medium was within 15 mg/ml.[17] Thus, the differences between RED_{raw} and RED_{cal} were within 10% at the concentration of the contrast medium used clinically. The accuracy of the RED_{cal} was within the SD value of the RED_{raw} for concentrations less than 10 mg/ml. Although the RED_{cal} could be useful for concentrations less than 10 mg/ml, the dose difference should be confirmed for concentrations over 10 mg/ml on radiotherapy treatment planning. A previous study reported the effect of intravenous contrast media on dose calculations in three-dimensional conformal radiation therapy (3D-CRT).[18] The dose differences between the planning image set using intravenous contrast and the image set without contrast showed an average increase in Monitor Units of 0.75–1.28%. Thus, the effect on dose from the contrast medium could be small in photon-based external radiotherapy.

Jang et al. reported that Lipiodol, which is used in transarterial chemoembolization (TACE), had a larger CT number, and its value was within 2000 HU.[19,20] The RED converted from the CT number, with a value around 2000 HU using the CT number–ED calibration table in Fig. 3 was approximately 1.8–2.0 g/cm^3 for 80 kV and 135 kV, respectively. A high-concentration contrast medium at over 20 mg/ml has been used for TACE. The RED_{cal} (Lung-bone) model was in good agreement, within 10%, compared with the other models in the 0–130 mg/ml range. The RED_{cal} (Lung-Ti and Lung-Ti with SEMAR) model included titanium, thereby the beam hardening artifact affected the CT number in titanium. The SEMAR algorithm reduced the metal artifact in titanium, and the accuracy of the RED_{cal} was improved. In the contrast medium, the RED should be increased as the concentration of the contrast medium is increased. The RED_{cal} with three models (Lung-Ti and Lung-Ti with SEMAR) at 130 mg/ml of the contrast medium was decreased compared with 90 mg/ml. Hence, the reconstruction image of the contrast medium at 130 mg/ml would be greatly affected by the metal artifact reduction. The CT number and RED of titanium were larger than the contrast medium. Therefore, the RED_{cal} (Lung-Ti and Lung-Ti with SEMAR) was definitely affected by the beam hardening artifact. Although the SEMAR algorithm reduces the beam hardening artifact around the materials with a higher density by excluding data in the metal trace region of the sinogram, it could not decrease artifacts in the materials with a higher density.

The limitation of the current study was that we did not evaluate how the difference of the RED caused the dose difference in radiation therapy treatment planning. However, a previous study revealed the dose difference in the case of varying relative RED.[21] Kilby et al. reported that the dose difference in prostate, breast, lung, and brain when increasing the relative RED by 3% for water and soft tissues, 5% for lung, and 8% for bone with 6- to 16-MV photon beams were within 1.7%. Therefore, the dose difference was small by comparison with the difference of the RED. The RED_{raw} and RED_{cal} values could be useful for radiation treatment planning. Especially, the RED_{raw} reduced the beam hardening artifact, and it could obtain high accuracy and precision, and did not need the CT numbers–RED or ΔHU–RED conversion or something similar.

5. Conclusion

The RED_{raw} data was highly accurate and precise in all tissue-equivalent inserts and the contrast medium at 0–130 mg/ml. The RED_{cal} values could be affected by beam hardening artifacts and the precision could be lower for low absolute CT numbers. The RED_{cal} data in the contrast medium is accurate at concentrations of contrast medium used in clinical practice.

Financial disclosure

None declared.

Conflict of interest

None declared.

REFERENCES

1. Ahnesjö A. Collapsed cone convolution of radiant energy for photon dose calculation in heterogeneous media. *Med Phys* 1989;**16**:577–92.
2. Garcia LI, Azorin JF, Almansa JF. A new method to measure electron density and effective atomic number using dual-energy CT images. *Phys Med Biol* 2016;**61**(1):265–79.
3. Parker RP, Hobday PA, Cassell KJ. The direct use of CT numbers in radiotherapy dosage calculations for inhomogeneous media. *Phys Med Biol* 1979;**24**(4):802–9.
4. Constantinou C, Harrington JC, DeWerd LA. An electron density calibration phantom for CT-based treatment planning computers. *Med Phys* 1992;**19**(2):325–7.
5. Fletcher JG, Leng S, Yu L, McCollough CH. Dealing with uncertainty in CT images. *Radiology* 2016;**279**:5–10.
6. Mileto A, Barina A, Marin D, et al. Virtual monochromatic images from dual-energy multidetector CT: variance in CT numbers from the same lesion between single-source projection-based and dual-source image-based implementations. *Radiology* 2016;**279**(Apr (1)):269–77.
7. Schneider U, Pedroni E, Lomax A. The calibration of CT Hounsfield units for radiotherapy treatment planning. *Phys Med Biol* 1996;**41**(1):111–24.
8. Maass C, Meyer E, Kachelriess M. Exact dual energy material decomposition from inconsistent rays (MDIR). *Med Phys* 2011;**38**(Feb (2)):691–700.
9. Saito M. Potential of dual-energy subtraction for converting CT numbers to electron density based on a single linear relationship. *Med Phys* 2012;**39**(4):2021–30.
10. Tsukihara M, Noto Y, Hayakawa T, Saito M. Conversion of the energy-subtracted CT number to electron density based on a single linear relationship: an experimental verification using a clinical dual-source CT scanner. *Phys Med Biol* 2013;**58**(9):N135–44.
11. Alvarez RE, Macovski A. Energy-selective reconstructions in X-ray computerized tomography. *Phys Med Biol* 1976;**21**:733–44.
12. Andersson KM, Nowik P, Persliden J, et al. Metal artefact reduction in CT imaging of hip prostheses—an evaluation of commercial techniques provided by four vendors. *Br J Radiol* 2015;**88**(Aug (1052)):20140473.
13. Meinel FG, Bischoff B, Zhang Q, et al. Metal artifact reduction by dual-energy computed tomography using energetic

extrapolation: a systematically optimized protocol. *Invest Radiol* 2012 Jul;**47**(7):406–14.
14. Miki K, Mori S, et al. Single-energy metal artefact reduction with CT for carbon-ion radiation therapy treatment planning. *Br J Radiol* 2016;**89**(Jun (1062)):20150988.
15. Lehmann LA, Alvarez RE, Macovski A, et al. Generalized image combinations in dual KVP digital radiography. *Med Phys* 1981;**8**(Sep–Oct (5)):659–67.
16. Torikoshi M, Tsunoo T, Sasaki M, et al. Electron density measurement with dual-energy X-ray CT using synchrotron radiation. *Phys Med Biol* 2003;**48**:673–85.
17. Bae KT. Intravenous contrast medium administration and scan timing at CT: considerations and approaches. *Radiology* 2010;**256**(Jul (1)):32–61.
18. Nasrollah J, Mikaeil M, Omid E, et al. Influence of the intravenous contrast media on treatment planning dose calculations of lower esophageal and rectal cancers. *J Cancer Res Ther* 2014;**10**(Jan–Mar (1)):147–52.
19. Fenster A. Split xenon detector for tomochemistry in computed tomography. *J Comput Assist Tomogr* 1978;(2):243–52.
20. Kawahara D, Ozawa S, et al. Dosimetric impact of lipiodol in stereotactic body radiation therapy on liver after trans-arterial chemoembolization. *Med Phys* 2017;**44**(Jan (1)):342–8.
21. Kilby W, Sage J, Rabett V. Tolerance levels for quality assurance of electron density values generated from CT in radiotherapy treatment planning. *Phys Med Biol* 2002;**47**(May (9)):1485–92.